Resolving surface chemical states in XPS analysis of first row transition metals, oxides and hydroxides: Sc, Ti, V, Cu and Zn

Mark C. Biesinger [a,b,*], Leo W.M. Lau [a,c], Andrea R. Gerson [b], Roger St.C. Smart [b]

[a] Surface Science Western, The University of Western Ontario, The University of Western Ontario Research Park, Room LL31, 999 Collip Circle, London, Ontario, Canada N6G 0J3
[b] ACeSSS (Applied Centre for Structural and Synchrotron Studies), University of South Australia, Mawson Lakes, SA 5095, Australia
[c] Department of Chemistry, The University of Western Ontario, London, Ontario, Canada N6A 5B7

ARTICLE INFO

ABSTRACT

Chemical state X-ray photoelectron spectroscopic analysis of first row transition metals and their oxides and hydroxides is challenging due to the complexity of the 2p spectra resulting from peak asymmetries, complex multiplet splitting, shake-up and plasmon loss structure, and uncertain, overlapping binding energies. A review of current literature shows that all values necessary for reproducible, quantitative chemical state analysis are usually not provided. This paper reports a more consistent, practical and effective approach to curve-fitting the various chemical states in a variety of Sc, Ti, V, Cu and Zn metals, oxides and hydroxides. The curve-fitting procedures proposed are based on a combination of (1) standard spectra from quality reference samples, (2) a survey of appropriate literature databases and/or a compilation of the literature references, and (3) specific literature references where fitting procedures are available. Binding energies, full-width at half maximum (FWHM) values, spin-orbit splitting values, asymmetric peak-shape fitting parameters, and, for Cu and Zn, Auger parameters values are presented. The quantification procedure for Cu species details the use of the shake-up satellites for Cu(II)-containing compounds and the exact binding energies of the Cu(0) and Cu(I) peaks. The use of the modified Auger parameter for Cu and Zn species allows for corroborating evidence when there is uncertainty in the binding energy assignment. These procedures can remove uncertainties in analysis of surface states in nano-particles, corrosion, catalysis and surface-engineered materials.

© 2010 Elsevier B.V. All rights reserved.

1. Introduction

Chemical state determination using X-ray photoelectron spectroscopy (XPS) has become routine for most of the elements in the periodic table. Binding energy (BE) databases, such as the NIST Database [1] or the Phi Handbook [2], generally provide sufficient data for the determination of chemical state for uncomplicated (i.e. single peak) spectra. However, the transition metal 2p spectra pose a number of problems that these databases do not adequately address, specifically, shake-up structure, multiplet splitting and plasmon loss structure, all of which can complicate both interpretation and quantitation of the chemical states present. For example, fitting parameters such as peak widths and asymmetries, which are vital for curve-fitting of complex, mixed metal/oxide systems, are not included in these databases.

The theoretical basis for multiplet, shake-up, plasmon loss and other contributions to the nickel metal, alloys, oxides and hydroxides has been discussed in our earlier paper [3] and in the extensive reviews by Hagelin-Weaver et al. [4,5]. The multiplet contributions can be based initially on the free ion case [6,7] but the more complex charge-transfer contributions from ligands currently being considered in several models [8,9] provide considerable theoretical and computational challenges. It is acknowledged that the current state of quantum modeling is not yet sufficient to reliably assign specific multiplet and shake-up contributions to allow calculation of the Ni 2p envelopes for each chemical state. Hence, quantitative fitting of different chemical states (e.g. Ni(II), Ni(III)) in these compounds has been necessarily semi-empirical. Practical methods to combine theoretical and experimental information to produce curve-fitting procedures have been developed and reported for Ni [3,10], Fe [11] and Cr [12] metal, oxides and hydroxides.

This paper surveys existing literature on chemical state identification and quantitative estimation from a variety of transition metal-containing materials of Sc, Ti, V, Cu and Zn. This information and our own measurements have been used to develop spectral curve-fitting procedures for determining chemical state information. The data used are based on one or a combination of (1) analysis

* Corresponding author at: Surface Science Western, The University of Western Ontario, The University of Western Ontario Research Park, Room LL31, 999 Collip Circle, London, Ontario, Canada N6G 0J3. Tel.: +1 519 661 2173; fax: +1 519 661 3709.
E-mail address: biesingr@uwo.ca (M.C. Biesinger).

Table 1
Spectral fitting parameters for Sc 2p species: binding energy (eV), FWHM value (eV) for each pass energy, and spectral component separation (eV).

Compound	Sc 2p$_{3/2}$ (eV)	Std. Dev. (±eV)	Sc 2p$_{1/2}$ (eV)	Std. Dev. (±eV)	Sc 2p$_{1/2}$–Sc 2p$_{3/2}$ splitting (eV)	FWHM (eV), 10 eV pass energy, Sc 2p$_{3/2}$	FWHM (eV), 10 eV pass energy, Sc 2p$_{1/2}$	FWHM (eV), 20 eV pass energy, Sc 2p$_{3/2}$	FWHM (eV), 20 eV pass energy, Sc 2p$_{1/2}$
Sc(0)[a]	398.45	0.02	403.19	0.02	4.74	0.64	0.72	0.76	0.79
Sc(III) oxide (powder)	401.71	0.09	406.16	0.09	4.45	1.15	1.54	1.18	1.57
Thin air-formed oxide/hydrated (ScOOH peaks)	402.97	0.11	407.46	0.08	4.49	1.71	2.18	1.71	2.16
Thick air-formed oxide/fully hydrated	402.87	0.05	407.45	0.07	4.58	1.86	2.30	1.87	2.27

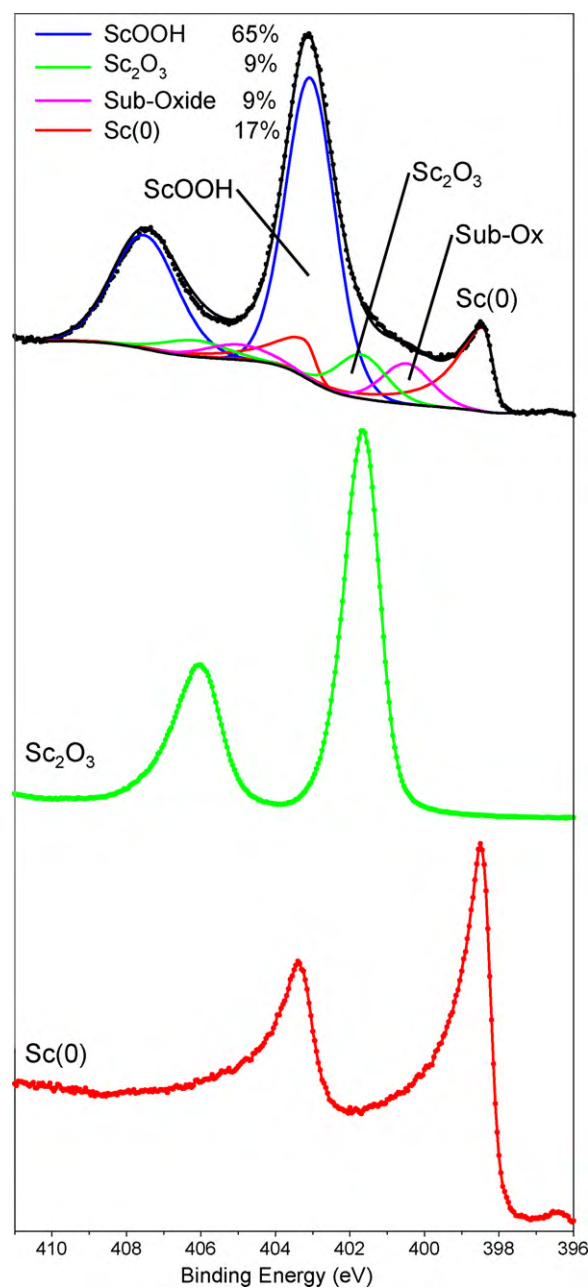[a] Asymmetric peak-shape LA(1.1,9,10).

Fig. 1. Sc 2p spectrum (top) of a thin, air-formed oxide (10 min laboratory air) formed on polished Sc metal using peak fittings derived from Table 1. The Sc 2p spectra for Sc$_2$O$_3$ (middle) and Sc metal (bottom).

of quality standard samples taken over the course of number of years on a state-of-the-art Kratos Axis Ultra XPS spectrometer, (2) a survey of the literature databases and/or a compilation of the literature references, and (3) specific literature references where fitting procedures are available. These procedures have been tested and validated on both synthetic and practical samples and have been found to be consistently reproducible across a wide range of samples (e.g. [13–15]).

We examine here Sc, Ti, V, Cu and Zn and their oxide and hydroxide compounds. Sc(III), Ti(IV), V(V), Cu(I), Cu(II) and Zn (II) species do not have unpaired d electrons and will not exhibit multiplet splitting. Ti(II), Ti(III), V(II), V(III) and V(IV) species have unpaired d electrons and should theoretically [6] exhibit mutiplet structure although in practice this may not be well resolved as found in previous XPS literature reports and our data from these compounds.

Table 2
Ti $2p_{3/2}$ literature values compiled from the NIST database [1] and selected literature references [30–32,34,53,54].

Compound	Ti $2p_{3/2}$ (eV)	Std. Dev. (±eV)	No. of citations	Ti $2p_{1/2}$–Ti $2p_{3/2}$ splitting (eV)	Std. Dev. (±eV)	No. of citations
Ti(0)	453.86	0.32	8	6.13	0.06	2
Ti(II) oxide	455.34	0.39	8	5.73	0.15	3
Ti(III) oxide	457.13	0.35	8	5.60	0.36	3
Ti(IV) oxide	458.66	0.22	13	5.66	0.08	4

Hence, fitting procedures for these compounds are more readily defined and more robust than those for other transition metal spectra. Some of our recent work has already shown that chemical state identification using improved multiplet structures can also lead to more accurate estimates of mixed species in thin films [10] compared with bulk nickel oxide/hydroxide surfaces [3,10]. In quantification of thin films by XPS, compositional and chemical state variation with depth can introduce significant errors, recently reviewed by Powell and Jablonski [16], due, in part, to inelastic mean free path (IMFP) differences associated with the different chemistries. Methods to explore layered structures (e.g. QUASES) [17] and evaluate multiphase particles [18] have been used in some of our previous work [3,10,19–22]. In this paper, we have focused on improved chemical state recognition and quantitative estimation. The procedures can be used in subsequent depth analysis [10,19]. Binding energy calibration procedures, essential to this process, particularly for sample charge referencing, are also described and discussed.

2. Experimental

The XPS analyses were carried out with a Kratos Axis Ultra spectrometer using a monochromatic Al Kα source (15 mA, 14 kV). The instrument work function was calibrated to give an Au $4f_{7/2}$ metallic gold binding energy (BE) of 83.95 eV. The spectrometer dispersion was adjusted to give a (BE) of 932.63 eV for metallic Cu $2p_{3/2}$. The Kratos charge neutralizer system was used for all analyses. Charge neutralization was deemed to have been fully achieved by monitoring the C 1s signal for adventitious carbon. A sharp main peak with no lower binding energy structure is generally expected. Instrument base pressure was 8×10^{-10} Torr. High-resolution spectra were obtained using an analysis area of ≈300 μm × 700 μm and either a 10 eV or 20 eV pass energy. These pass energies correspond to Ag $3d_{5/2}$ FWHM of 0.47 eV and 0.55 eV, respectively.

A single peak (Gaussian (70%)–Lorentzian (30%)), ascribed to alkyl type carbon (C–C, C–H), was fitted to the main peak of the C 1s spectrum for adventitious carbon. A second peak is usually added that is constrained to be 1.5 eV above the main peak, and of equal FWHM to the main peak. This higher BE peak is ascribed to alcohol (C–OH) and/or ester (C–O–C) functionality. Further high BE components (e.g. C=O, 2.8–3.0 eV above the main peak, O–C=O, 3.6–4.3 eV above the main peak) can also be added if required. Spectra from insulating samples have been charge corrected to give the adventitious C 1s spectral component (C–C, C–H) a BE of 284.8 eV. The process has an associated error of ±0.1–0.2 eV [23]. Experience with numerous conducting samples and a routinely calibrated instrument has shown that the non-charge corrected C 1s signal generally ranges from 284.7 eV to as high as 285.2 eV [24]. The spectra for all (argon ion sputter cleaned) metallic species are referenced to Au $4f_{7/2}$ at 83.95 eV. The powder (or consolidated) samples were not sputter cleaned prior to analysis, as it is well known that this can cause reduction of oxidized species.

Spectra were analyzed using CasaXPS software [25] (version 2.3.14). Gaussian (Y%)–Lorentzian (X%), defined in CasaXPS as GL(X), profiles were used for each component. The best mixture of Gaussian–Lorentzian components will vary depending on the instrument and resolution (pass energy) settings used as well as on the natural line-width of the specific core hole. For example, on this instrument at 10 eV and 20 eV pass energies, the Ti 2p lines for titanium dioxide are best fit with line-shapes of GL(69) and GL(67), the V 2p line for V_2O_5 fit best with GL(90) and GL(82), and the Sc 2p lines for Sc_2O_3 fit best with GL(59) and GL(52). The C 1s and O 1s lines, which have a larger natural line-widths, are better fit with a GL(30) line-shape. Changes to the Gaussian–Lorentzian mix do not, in general, constitute large peak area changes in fitting of mixed oxide systems (with the metal component being the exception). As long as the mix is in a reasonable range and applied consistently, reasonable results are obtained.

For metallic core lines, asymmetry was defined in the form of LA(α, β, m) where α and β define the spread of the tail on either side of the Lorentzian component. The parameter m specifies the width of the Gaussian used to convolute the Lorentzian curve. If values of α and β greater than unity are used this line-shape will correct a problem with previous asymmetric line-shapes [3,11,12] that tend to incorrectly estimate the peak area by incorporating area under the curve from binding energies well above the peak profile [26]. A standard Shirley background is used for all reference sample spectra.

Powder and metal samples of the highest purity readily available were purchased from Alfa Aesar. Where available, samples that were received ampouled under argon were introduced into the XPS instrument via an attached argon filled glove box (VO, VO_2). Samples obtained in consolidated form (V_2O_5) were fractured in vacuum prior to analysis. All powder samples were mounted on non-conductive adhesive tape. Metallic samples were sputter cleaned using a 4 kV argon ion beam to remove all oxide and carbonaceous species. Sc_2O_3, V_2O_5, VO_2, V_2O_3, VO, Cu_2O, $Cu(OH)_2$, CuO and ZnO samples were checked for purity by powder X-ray diffraction (XRD) using an Inel diffractometer equipped with a XRG 3000 generator and CPS 120 curved position sensitive detector using monochromated Cu Kα radiation (λ = 1.54056 Å). TiO_2 (anatase and rutile) samples were checked for purity by Raman spectroscopy analysis using a Renishaw 2000 Laser Raman spectrometer. XPS survey scan (elemental) data from these standards are presented in Appendix I.

Powder and polycrystalline materials were used to remove the possibility of photoelectron diffraction effects, which can influence splitting patterns [27,28]. They are also more representative of the majority of samples in practical analyses of air-exposed multi-component materials.

3. Results and discussion

3.1. Scandium

Relatively little XPS analysis of Sc and its oxides has been completed beyond the reporting of BE values taken of the metal and pure oxide (Sc_2O_3) [1,2]. This is presumably due to its relative rarity and low level of industrial use. The XPS data from Sc metal and its oxide, Sc_2O_3, which has no unpaired electrons, can be simply fitted with a doublet of appropriately constrained peaks. Peak fitting

Table 3
Spectral fitting parameters for Ti 2p species: binding energy (eV), FWHM value (eV) for each pass energy, and spectral component separation (eV).

Compound	Ti 2p$_{3/2}$ (eV)	Std. Dev. (±eV)	Ti 2p$_{1/2}$ (eV)	Std. Dev. (±eV)	Ti 2p$_{1/2}$–Ti 2p$_{3/2}$ splitting (eV)	FWHM (eV), 10 eV pass energy, Ti 2p$_{3/2}$	FWHM (eV), 10 eV pass energy, Ti 2p$_{1/2}$	FWHM (eV), 20 eV pass energy, Ti 2p$_{3/2}$	FWHM (eV), 20 eV pass energy, Ti 2p$_{1/2}$
Ti(0)[a]	453.74	0.02	459.79	0.03	6.05	0.59	0.78	0.69	0.83
Ti(IV) oxide (rutile)	458.46	0.09	464.23	0.13	5.77	0.99	1.97	1.04	2.01
Ti(IV) oxide (anatase)	458.59	0.00	464.31	0.00	5.72	0.98	1.97	1.04	1.98

[a] Asymmetric peak-shape LA(1.1.5.7).

parameters for Sc 2p spectra are presented in Table 1. The Sc 2p$_{1/2}$ peak for each species is constrained to be at a fixed energy increment above the Sc 2p$_{3/2}$ peak. The intensity ratio of the Sc 2p$_{3/2}$ and Sc 2p$_{1/2}$ peaks is constrained to 2:1. This is consistent with the expected ratio of $(2j_1 + 1)/(2j_2 + 1)$, where j_1 and j_2 represent the coupled orbital (l) and spin (s) angular momentum quantum numbers from respective spin-up and spin-down states of the unpaired core electron subsequent to photoionization. The Sc 2p$_{3/2}$ XPS BE peak for the metal is at 398.45 eV and is fitted with an asymmetric peak-shape (Fig. 1).

The Sc 2p$_{3/2}$ BE for the pure oxide standard is at 401.7 eV (Fig. 1) with a main O 1s peak at 529.7 eV (FWHM ≈ 1 eV) indicative of a lattice oxide. This is in good agreement with the literature values [1]. There is also a second O 1s peak at approximately 1.6 eV above the main peak (≈2.0 eV FWHM) that constitutes 25–30% of the total O 1s envelope. This peak may be ascribed to defective sites in the oxide or to hydroxide functionality (probably a mix of both). A small amount of organic oxygen, normally C–O–C, will also be present in the adventitious hydrocarbon overlayer.

In contrast, the thick air-formed oxide (formed over a period of years) has a Sc 2p$_{3/2}$ BE of 402.9 eV and a broader O 1s (FWHM ≈ 2.6 eV) peak at 531.8 eV indicative of hydroxide and hydrated species. A thin, air-formed oxide (10 min laboratory air), on polished Sc metal (Fig. 1), was collected without the aid of charge neutralization and has been described as an insoluble hydrous oxide (ScO(OH)) [29]. The intermediate structure between the metal and ScO(OH) peak can be explained by the oxide (doublet of peaks set at 3.16 eV above the metal doublet), and by the formation of a thin sub-oxide layer at the oxide/metal interface. From the fitting of the O 1s spectrum, an approximately 1.3:1 oxide to hydroxide ratio is obtained which incorporates a combination of the oxy-hydroxide, oxide and sub-oxide species. A small amount of adsorbed water was also detected.

3.2. Titanium

Ti 2p$_{3/2}$ spectral fitting parameters compiled from the NIST database [1] and selected literature references are presented in Table 2. As with the NIST database, this survey of BE averages (with standard deviations and number of references) obtained from a large database of published work is valuable for several reasons. It is possible to identify BE values in good agreement (i.e. large number of references, small standard deviation), BE values in dispute or less reliable (i.e. large standard deviation) and BE values relatively unknown (with few or no references), which should be verified by analysis of standard samples.

Numerous papers report the BE for Ti metal and Ti(IV) oxides [30–35]. Godfroid et al. [31] correctly use an asymmetric peak-shape to represent the Ti metal peak and provide details of peak positions while following thin film Ti oxide growth. Pouilleau et al. [32] present spectra and BE values for their analysis of passive Ti oxide films, but do not take into account charge referencing making the values presented difficult to apply. McCafferty and Wightman [33] report values from a survey of the literature and apply them to a study of native air-formed Ti oxide films. The adventitious C 1s set to 285.0 eV is used for charge referencing. Charge referencing to the well-characterized Ti(IV) oxide (TiO$_2$) at 458.5 eV is proposed by González-Elipe et al. [30] and others [33,34].

Whereas the Ti 2p$_{3/2}$ peak positions for Ti(IV) and Ti metal are in good agreement across the various studies, the evidence for and assignment of the exact BE peak positions for Ti(II) and Ti(III) oxides is less convincing. Balaceanu et al. [36] incorrectly assign Ti$_2$O$_3$ to a Ti 2p$_{3/2}$ peak at 458.5 eV. The authors incorrectly reference this value to González-Elipe et al. [30]. González-Elipe et al. [30] give BE values for Ti$_2$O$_3$ and TiO based on argon ion sputter reduced samples. Massaro et al. [37] also charge correct to the Ti(IV) peak

Table 4
V 2p$_{3/2}$ literature values (compiled from Ref. [1]).

Compound	V 2p$_{3/2}$ (eV)	Std. Dev. (±eV)	No. of citations	V 2p$_{1/2}$–V 2p$_{3/2}$ splitting (eV)	Std. Dev. (±eV)	No. of citations
V(0)	512.43	0.24	10	7.62	0.06	5
V(III) oxide	515.35	1.58	4			
V(III) hydroxide	514.10		1			
V(IV) oxide	516.30	0.42	3			
V(V) oxide	517.26	0.64	23	7.48		1

set to 458.5 eV, but use a single peak set between 456.0 eV and 456.3 eV to represent both Ti(II) and Ti(III) species.

Smith and Henrich [38] present an analysis of a Ti$_2$O$_3$ surface and show its 2p spectrum to be broadened with structure present on the lower BE side of the main peak at 459.6 eV. They suggest the surface has been oxidized in the presence of SO$_2$ to TiO$_2$ and TiS$_2$ although the BE values given do not necessarily support this (the authors reference TiO$_2$ at 458.9 eV and TiS$_2$ at 454.6 eV). Unfortunately the authors do not present the Ti 2p spectrum for an unexposed Ti$_2$O$_3$ surface.

Botha's [39] analysis of Ti$_2$O$_3$ coated bio-implants reports a single peak for Ti$_2$O$_3$ with small amounts of TiO and Ti metal. However, the spectrum shown is not corrected for charging and could have resulted from TiO$_2$, with small amounts of Ti$_2$O$_3$ and TiO. Although the author has stated that a 15 Å layer of gold has been added as a charge reference, BE values for the Ti 2p$_{3/2}$ spectra are not given.

Hudson et al. [40] report a broadened structure with a clearly defined peak on the lower BE side of the main peak for a Ti 2p$_{3/2}$ spectrum of vacuum fractured Ti$_2$O$_3$. They attribute this to "unresolved Ti 2p components attributed to well-screened and poorly screened core holes." This is referenced to unpublished results of Kurtz (one of the authors) and Henrich. Nasser [35] also references Kurtz's work [41] that showed UHV-cleaved Ti$_2$O$_3$ to have a complex line-shape arising from final state screening effects. Ti$_2$O$_3$ reference spectra from UHV-cleaved single crystal Ti$_2$O$_3$ have been published [42,43]. Ti(III) has one unpaired electron in the valence shell ([Ar]3d^1) and Ti(II) has two unpaired electrons in the valence shell ([Ar]3d^2). Calculations by Gupta and Sen [6] confirm that there is some multiplet structure associated with Ti (II) and Ti (III) free ions. The structures reported [41,42] may be associated with this. It is also possible that the structure reported may be due to chemical state differences at the surface of the Ti$_2$O$_3$ crystal.

The literature provides numerous examples [44–51] of studies involving single crystal TiO$_2$. However, generally these involve the adsorption of compounds on specific anatase or rutile surfaces (faces) and are focused on the chemistry taking place and not on XPS fitting or quantification procedures beyond mentioning the Ti 2p$_{3/2}$ BE position. It is relatively rare to find full disclosure of FWHM or Ti 2p$_{1/2}$–2p$_{3/2}$ splitting values. Older data also tends to have been taken with non-monochromatic X-ray sources and displays broader FWHM than more modern data recorded with today's high-

resolution monochromatic sources. Sputtered single crystal TiO$_2$ results from Hashimoto et al. [52] show a convincing peak for Ti(III) at 456.6 eV with a second component at 454.4 eV ascribed to Ti(II) species (charge corrected to C 1s = 284.6 eV). No fitting parameters are presented.

No XPS analysis for a standard sample of TiO could be found. In addition, peak widths are generally not reported for all Ti species beyond noting that the Ti 2p$_{1/2}$ peak is broader than the Ti 2p$_{3/2}$ peak.

Our initial fitting parameters for Ti 2p spectra were developed using averaged BE data and 2p$_{1/2}$–2p$_{3/2}$ splitting data from the NIST XPS Database [1] and selected literature references [30–32,34,53,54] (Table 2). As well, data from readily available standard samples (metal, TiO$_2$) were used to clarify the peak widths, doublet splitting (Δ = 6.05 eV for Ti(0), Δ = 5.72 eV for Ti(IV)) and shapes (asymmetric for the metallic component) (Table 3).

An example of the use of these parameters is presented for a mixed oxidation state Ti-containing sample in Fig. 2. Although C 1s set to 284.8 eV can be used as an internal charge correction it is also possible in this case to use the Ti 2p$_{3/2}$ metal peak set at 453.7 eV or the clearly defined Ti(IV) (TiO$_2$) 2p$_{3/2}$ peak set at 458.6 eV. This removes the uncertainty associated with charge correcting to adventitious C especially in situations where the adventitious overlayer is not in good electrical contact with the Ti-containing species underneath. The Ti 2p$_{1/2}$ peak for each species is constrained to be at a fixed energy above the Ti 2p$_{3/2}$ peak. The intensity ratio of the Ti 2p$_{3/2}$ and Ti 2p$_{1/2}$ peaks is also constrained to be 2:1. The FWHM values for the metal and Ti(IV) peaks are derived from the standard sample analyses. The FWHM values for Ti(II) (at a BE of 455.3 eV) and Ti(III) (at a BE of 457.1 eV), which are likely structurally loosely ordered, are constrained to have equal widths, and are generally slightly broader than the well ordered Ti(IV) oxide peaks. In applications when adventitious C is used as a charge reference the quoted binding energies are allowed to vary by ±0.1–0.2 eV in accordance with the uncertainty associated with this method.

3.3. Vanadium

Table 4 lists the V 2p$_{3/2}$ BE and V 2p$_{3/2}$–V 2p$_{1/2}$ splitting values from a survey of the literature sources compiled in the NIST Database [1]. Silversmit et al. [50,55,56] provide a nearly complete set of fitting parameters for V 2p spectra. The results obtained

Table 5
Spectral fitting parameters for V 2p species: binding energy (eV), FWHM value (eV) for each pass energy, and spectral component separation (eV) from Refs. [55–57]. Binding energy values are corrected to oxygen 1s set to 530.0 eV.

Compound	V 2p$_{3/2}$ (eV)^c	Std. Dev. (±eV)	V 2p$_{1/2}$–V 2p$_{3/2}$ splitting (eV)	FWHM (eV), V 2p$_{3/2}$, single species^a	FWHM (eV) V 2p$_{1/2}$, single species^a	FWHM (eV), V 2p$_{3/2}$, mixed oxide^b	FWHM (eV), V 2p$_{1/2}$, mixed oxide^b
V(0)	512.35	0.20	7.50			0.9–1.3	1.3–1.7
V(I) and/or V(II)	513.67	0.20	7.33			2.0–2.3	2.6–3.4
V(III) oxide	515.29	0.20	7.33	3.3–3.4	4.0–4.4	2.7–4.0	3.1–4.7
V(IV) oxide	515.84	0.20	7.33	1.2	2.6–3.0	2.2–3.2	3.1–3.7
V(V) oxide	517.20	0.10	7.33	0.9^d	2.4^d	1.0–1.5	2.6

^{a} Peak widths from standard vanadium oxide compounds.
^{b} Peak widths from a fitting of mixed (sputter etched) vanadium oxides.
^{c} Corrected to E(Fermi).
^{d} Using a pass energy of 5.85 eV, all others spectra taken with a pass energy of 11.75 eV (lower resolution than 5.85 eV).

Table 6
Spectral fitting parameters for V 2p species: binding energy (eV), FWHM value (eV) for each pass energy, and spectral component separation (eV).

Compound	V 2p$_{3/2}$ (eV)	Std. Dev. (±eV)	V 2p$_{1/2}$ (eV)	Std. Dev. (±eV)	V 2p$_{1/2}$–V 2p$_{3/2}$ splitting (eV)	FWHM (eV), 10 eV pass energy, V 2p$_{3/2}$	FWHM (eV), 10 eV pass energy, V 2p$_{1/2}$	FWHM (eV), 20 eV pass energy, V 2p$_{3/2}$	FWHM (eV), 20 eV pass energy, V 2p$_{1/2}$
V(0)	512.22	0.02	519.75	0.02	7.53	0.77	1.11	0.83	1.16[a]
V(IV) oxide	516.35	0.07			7.35[b]	1.37			
V(V) oxide	517.91	0.11	525.26	0.13	7.35	0.94	2.47	1.01	2.49

[a] Asymmetric peak-shape LA(1.2.5.8).
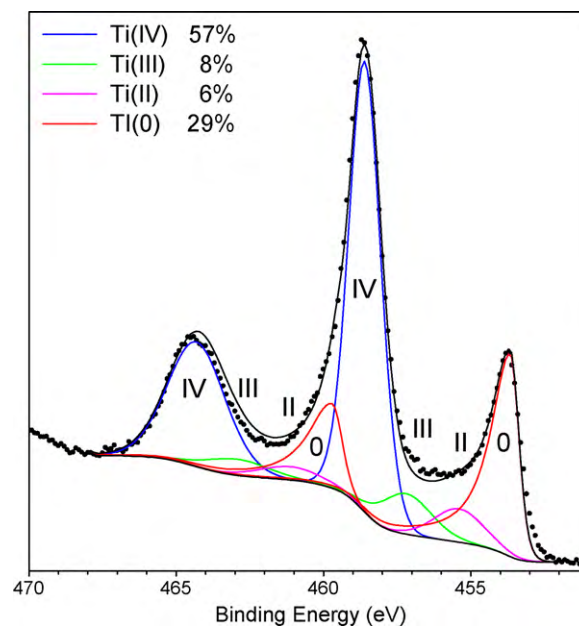[b] Based on V(V) splitting.

Fig. 2. Ti 2p spectrum of a heat-treated Ti-apatite composite using peak fittings derived from Tables 2 and 3.

are based on spectra from a series of standard samples including V$_2$O$_5$ (single crystal cleaved in vacuum), VO$_2$ (2 separately supplied powders pressed into a pellet, argon ion sputtered), and V$_2$O$_3$ (powder pellet, argon ion sputtered) using a Perkin-Elmer Phi ESCA 5500 equipped with a monochromatic Al Kα source. O 1s (set at 530.0 eV) is used as a BE reference and is included in the spectrum for the determination of the Shirley background underneath the V 2p region. The authors give FWHM values for both V 2p$_{3/2}$ and 2p$_{1/2}$ for V$_2$O$_5$ and VO$_2$, but do not provide FWHM values for other species. However subsequent correspondence with the author [57] provided further FWHM details and these are provided in Table 5. Similar to Ti 2p$_{1/2}$ peak, the V 2p$_{1/2}$ peak is broadened compared to the V 2p$_{3/2}$ due to the Coster–Kronig effect [56]. This effect is described as a special form of the Auger process in which the core hole in a shell with a certain principal quantum number is rapidly filled by an electron from a higher-energy shell of the same principal quantum number. Coster–Kronig processes are very fast, on the order of 10^{-15} s, and produce broad peak-shapes [58]. While V(V) species do not have unpaired valence electrons and thus show a sharp single line-shape, V(IV) and V(III) should and do exhibit some multiplet structure. This [55,56] and other papers [51,59,60] do not attempt to address this multiplet structure and only indicate broadening of the V(IV) and V(III) components.

Kurmaev et al. [61] in their single crystal studies of VO$_2$ present both V 2p$_{3/2}$ and V 2p$_{1/2}$ BE values (515.95 eV and 523.48 eV) and FWHM values (2.04 eV and 2.56 eV) with an O 1s value of 529.75 eV (1.30 eV FWHM). Youn et al. [62] report full V 2p$_{3/2}$ peak parameters for V$_2$O$_5$, VO$_2$ and V$_2$O$_3$ containing films on amorphous SiO$_2$/Si surfaces. BE (FWHM) values for V$_2$O$_5$ range from 515.92 eV to 516.22 eV (1.18–1.32 eV), VO$_2$ ranges from 514.95 eV to 515.31 eV (1.03–1.25 eV), and V$_2$O$_3$ ranges from 514.03 eV to 514.34 eV (1.13–1.36 eV). All values are referenced to C 1s at 284.6 eV.

Table 6 presents V 2p peak fitting parameters taken from our reference sample analyses. The spectra for V(IV) oxide showed a considerable amount of V(V) oxide to also be present (presumably from air oxidation of the surface of the samples). Spectra from V(III) samples (shown to be pure V$_2$O$_3$ by XRD) were surface oxidized to

Table 7
Cu $2p_{3/2}$ and modified Auger parameter literature values for Cu species (compiled from Ref. [1]).

| Compound	Cu $2p_{3/2}$ (eV) (Lit. Ave)	Std. Dev. (±eV)	No. of citations	Modified Auger parameter (Lit. Ave.)	Std. Dev. (±eV)	No. of citations
Cu(0)[a]	932.61	0.21	27	1851.23	0.16	23
Cu(I) oxide	932.43	0.24	18	1849.19	0.32	10
Cu(II) oxide[b]	933.57	0.39	18	1851.49	0.35	10
Cu(II) hydroxide[b]	934.75	0.50	2			

[a] *Note*: The ISO calibration standard is to set Cu $2p_{3/2}$ for the metal to 932.63 eV.
[b] Must show shake-up peaks.

V(IV) and V(V) species (making them unsuitable for use here) while spectra from a V(II) oxide sample showed the metal and a mix of oxide species. While peak widths for the metal and V(V) oxide are quite narrow (0.77 eV and 0.91 eV, respectively, for a 10 eV pass energy), the peak widths for V(III) and V(IV) oxides are considerably broadened. This is not unexpected as multiplet splitting should be occurring for these compounds as predicted by Gupta and Sen [6]. However, the spectra are not resolved into specific components as predicted by Gupta and Sen's calculations. This may be clarified if suitably pure V(III) and V(IV) (and V(II)) standards can be produced. V(V) has no unpaired electrons and as such will not show any multiplet splitting.

The BE values presented in Table 5 are charge corrected to O 1s set to 530.0 eV while the values in Table 6 are corrected to C 1s at 284.8 eV. If the spectra from the reference samples analyzed here are corrected to O 1s at 530.0 eV, very similar values are obtained (e.g. V $2p_{3/2}$ for V(V) at 517.16 ± 0.01 eV and V(IV) at 515.6 ± 0.07 eV from this work compared to 517.2 eV and 515.8 eV for Silversmit et al.). An average of NIST database [1] values for the O 1s signal for V_2O_5 gives a BE of 530.26 ± 0.32 eV. Correction to O 1s only works when the bulk of the sample is a vanadium oxide. In systems where vanadium is a minor oxide component, charge correction to adventitious carbon would be a superior choice. Alternatively, it may also be possible to correct to a strong V(V) peak or a well-defined V(0) peak if they are present. Charge correction to these peaks should be more reliable than the C 1s signal.

Peak fitting parameters assembled from the three sets of data (Tables 4, 5 and 6) were used to fit the spectra shown in Fig. 3 from the V(II) oxide sample clearly showing it is a mix of species. A Shirley background extended to include the O 1s portion of the spectrum is used and appears to give a reasonable result except for a slight 'underfitting' of the $2p_{1/2}$ portion of the spectrum (i.e. some peak area is not accounted for). If a Shirley background is applied across only the V 2p portion of the spectrum a much more severe 'overfit' of $2p_{1/2}$ portion of the spectrum is found. On comparison of a number of different V samples it appears that the previous option is preferable. It may be possible using a background offset on the higher BE portions to further improve the fit of the $2p_{1/2}$, however the improvement in quantification, based on the $2p_{3/2}$ spectrum, will be marginal at best.

It should also be noted that V_2O_5 degrades slowly under the X-ray beam to V(IV) compounds. Using a 210 W source (15 mA, 14 kV)
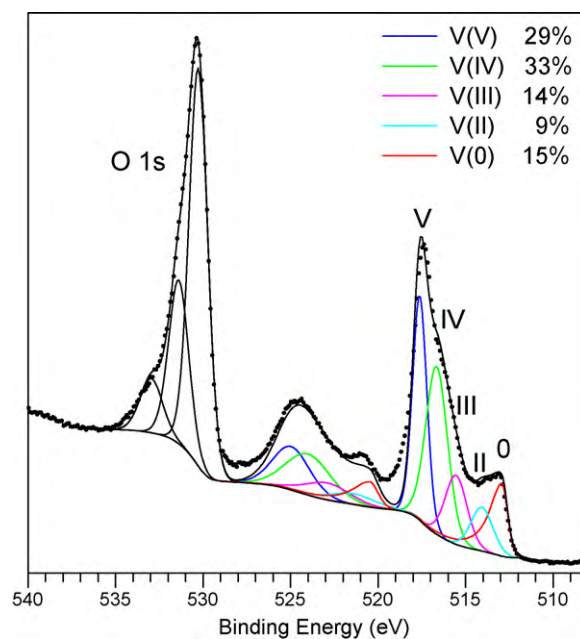
Fig. 3. V 2p (and O 1s) spectrum of a mixed vanadium oxide sample.

and a timed set of scans, more than 15% conversion of V(V) to V(IV) was found over a 24 h period. This should also be taken into account during any analysis of V compounds.

3.4. Copper

Table 7 lists Cu $2p_{3/2}$ BE and modified Auger parameter values from a survey of the literature sources compiled in the NIST Database [1]. Of note here is the statistically similar BE values for the Cu metal and Cu(I) oxide species. The use of the modified Auger parameter ($2p_{3/2}$, $L_3M_{45}M_{45}$) as well as an inspection of the Auger peak-shape do allow for a more accurate assignment for these species and has been used effectively. Goh et al. [63] have shown (in their Figure 8) the distinctly different peak-shapes of the X-ray generated Auger LMM spectra for copper as the metal, Cu_2S and CuS. They also note the distinctive Cu $L_3M_{4,5}M_{4,5}$ peak at 916.5 eV for Cu_2O. Poulston et al. [64], in their study of surface oxidation

Table 8
Cu $2p_{3/2}$ and modified Auger parameter values for Cu species from this work.

Compound	Cu $2p_{3/2}$ (eV)	Std. Dev. (±eV)	FWHM (eV), 10 eV pass energy	FWHM (eV), 20 eV pass energy	Modified Auger parameter (eV)	Std. Dev. (±eV)
Cu(0)	932.63[a]	0.025[b]	0.79	0.83	1851.24	0.025[b]
Cu(I) oxide	932.18	0.12	0.88	0.98	1849.17	0.03[c]
Cu(II) oxide[d]	933.76	0.11	3.00	3.00	1851.33	0.05[e]
Cu(II) hydroxide[d]	934.67	0.02	2.74	2.85	1850.92	0.09[e]

[a] ISO Calibration Standard 932.63 eV, GL(90) peak-shape.
[b] As defined by Kratos calibration procedure.
[c] GL(90) peak-shape.
[d] Shake-up peaks are present (see Fig. 4).
[e] GL(30) peak-shape.

Table 9
Cu 2p$_{3/2}$ fitting parameters for Cu(II) species.

Compound	Peak 1 (eV)	%	Δ Peak 2–peak 1 (eV)	FWHM (eV), 20 eV pass energy[a]	Peak 2 (eV)	%	Δ Peak 3–peak 2 (eV)	FWHM (eV), 20 eV pass energy	Peak 3 (eV)	%	Δ Peak 4–peak 3 (eV)	FWHM (eV), 20 eV pass energy	Peak 4 (eV)	%	Δ Peak 5–peak 4 (eV)	FWHM (eV), 20 eV pass energy	Peak 5 (eV)	%	FWHM (eV), 20 eV pass energy
Cu(II) oxide	933.11	31	1.37	2.07	934.48	33	6.04	1.03	940.52	3	1.13	3.55	941.66	28	2.05	1.17	943.71	6	
Cu(II) hydroxide	934.67	60	4.63	2.85	939.30	6	2.90	3.66	942.20	28	1.92	1.76	944.12	7					

[a] GL(30) peak profiles for all peaks.
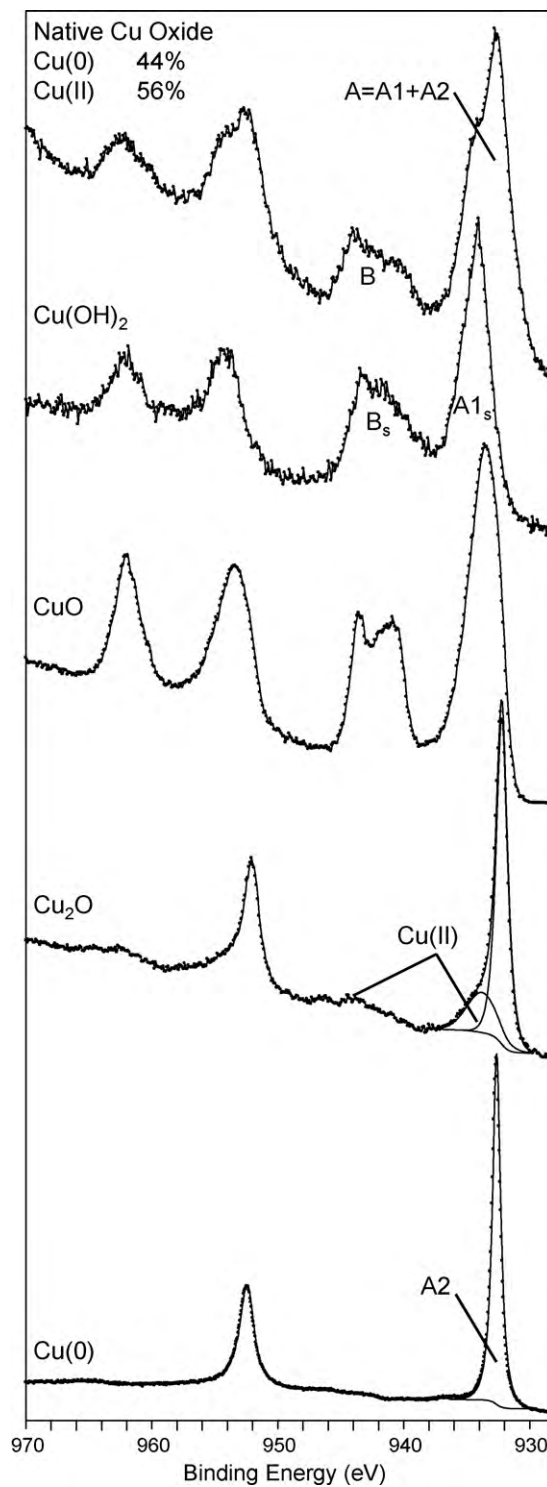
Fig. 4. Cu 2p spectra for a sputter cleaned Cu metal surface (bottom), Cu$_2$O standard (2nd from bottom, a small amount of Cu(II) was found in this sample), CuO standard (3rd from bottom), Cu(OH)$_2$ standard (4th from bottom) used for $A1_s/B_s$ determination and a spectrum of a native oxide on a metal surface (top) with the proportion of Cu(0) and Cu(II) calculated.

and reduction of Cu$_2$O and CuO, have used both the Cu LMM and the Auger parameter to distinguish Cu(0), Cu(I) and Cu(II). These parameters are very useful for the identification of the different states present in the surface but they are difficult to quantify as relative amounts of each species. The Cu 2p XPS spectrum is still the signal most used for this purpose.

Table 8 shows similar results to those shown in Table 7 from our work for a series of standard samples. In this analysis, a statistical separation of the Cu 2p$_{3/2}$ peak position for Cu(0) and Cu$_2$O is achieved. This should be expected, as most spectrometer calibration procedures include referencing to the ISO standard Cu metal line at 932.63 eV with deviation of this line set at ±0.025 eV. Curve-fitting of the Cu 2p$_{3/2}$ line for both Cu metal and Cu$_2$O employed Gaussian (10%)–Lorentzian (90%) p and Gaussian (20%)–Lorentzian (80%) peak-shapes, respectively (defined in CasaXPS as GL(90) and GL(80)). Peak-fit for these species are shown in Fig. 4.

Many authors use the presence of the well known shake-up satellite found in Cu 2p spectra as an indication of the presence of Cu(II) species [64–71]. Some choose to use this information in only a qualitative fashion [64–67]. Others taking a quantitative approach have peak fit the main 2p$_{3/2}$ peak with two to three separate components, the metal, Cu(I) and Cu(II), but ignore the contribution of the shake-up satellite [68,69]. Kundakovic and Flytzani-Stephanopoulos [70] use the presence of the shake-up peak to estimate the amount of CuO, but do not elaborate on the method by which the amounts given are obtained. Salvador et al. [71] use ratios of the main 2p$_{3/2}$ peak to the shake-up peak to qualitatively compare the amount of oxidation of copper in YBa$_2$Cu$_3$O$_{7-x}$ samples to a fully oxidized CuO standard sample.

Recently, a study of the surface chemistry of the flotation separation of chalcocite (Cu$_2$S) from heazelwoodite (Ni$_3$S$_2$) employed a fitting procedure and calculation that quantifies the amount of Cu(II) species present on the surface of Cu(I) sulfide [72] as first developed by Jasieniak and Gerson (2004) and now described in Ref. [73]. The calculation takes into account the photoelectron yield from both the main 2p$_{3/2}$ peak and the shake-up peak and is based on main peak/shake-up peak ratios derived from Cu(OH)$_2$ standard spectra. X-ray reduction of the Cu(II) samples has also been considered in this work.

Quantification of the amount of Cu(II) species on a Cu(0) or Cu(I) containing surface does appear to be possible. If, for example, a Cu metal surface is oxidized to Cu(II), the shake-up structure associated with the Cu(II) species can be used for a Cu(0):Cu(II) quantification. Alternatively if Cu(II) species and Cu(I) species are present, the Cu(I):Cu(II) ratio can be determined. This method [72] of Cu(0):Cu(II) (or Cu(I):Cu(II)) determination depends on shake-up peaks that are present in the spectra of d^9 Cu(II) containing samples but are absent in d^{10} Cu(0) (or Cu(I)) spectra. Shake-up peaks may occur when the outgoing photoelectron simultaneously interacts with a valence electron and excites it to a higher-energy level. The kinetic energy of the shaken-up core electron is then slightly reduced giving a satellite structure a few eV below (higher on the calculated BE scale) the core level position [74]. Hence, these electrons are part of the total Cu 2p emission and should be included in both total Cu and relative chemical state speciation. For example, the main emission line (A) in Fig. 4 contains both Cu(II) (A1) and Cu(0) (A2) contributions but the satellite intensity (B) is entirely from Cu(II). The total intensity from Cu(II) species is represented in the combination of the signals from the direct photoemission (A1) and the shaken-up photoemission (B).

Accurate Cu(0):Cu(II) ratios for samples containing a mixture of Cu(0) and Cu(II) rely on determining an accurate ratio of the main peak/shake-up peak areas ($A1_s/B_s$) for a 100% pure Cu(II) sample. With a reliable value of $A1_s/B_s$ obtained for Cu(OH)$_2$ or CuO (where all copper present is in the Cu(II) state), the relative concentrations of Cu(0) and Cu(II) species present on a surface that contains both species can be obtained by the following simple equations:

$$\% \ Cu(0) = \frac{A2}{A+B} \times 100 = \frac{A-A1}{A+B} \times 100 = \frac{A-(A1_s/B_s)B}{A+B} \times 100 \quad (1)$$

Table 10
Zn 2p$_{3/2}$, Zn 2p$_{1/2}$ and modified Auger parameter values for Zn species: FWHM value (eV) for each pass energy, and spectral component separation as well as Zn 2p$_{3/2}$ and modified Auger parameter literature values (compiled from Ref. [1]).

Compound	Zn 2p$_{3/2}$ (eV)	Std. Dev. (±eV)	Zn 2p$_{1/2}$ (eV)	Std. Dev. (±eV)	Zn 2p$_{1/2}$–Zn 2p$_{3/2}$ splitting (eV)	FWHM (eV), 10 eV pass energy, Zn 2p$_{3/2}$	FWHM (eV), 10 eV pass energy, Zn 2p$_{1/2}$	FWHM (eV), 20 eV pass energy, Zn 2p$_{3/2}$	FWHM (eV), 20 eV pass energy, Zn 2p$_{1/2}$	Modified Auger parameter (eV)	Zn 2p$_{3/2}$ (Lit. Ave)	Std. Dev. (±eV)	No. of citations	Modified Auger parameter (eV) (Lit. Ave.)	Std. Dev. (±eV)	No. of citations
Zn(0)[a]	1021.65	0.01	1044.66	0.01	23.01	0.82	1.00	0.86	1.04	2013.77	1021.62	0.38	15	2013.85	0.25	13
Zn(II) oxide	1021.00	0.04	1044.11	0.04	23.11	1.55	1.59	1.60	1.63	2010.40	1021.96	0.53	16	2010.14	0.39	9

[a] Asymmetric peak-shape LA(1.4.2.2).

Table 11
Selected O 1s values.

Compound	O 1s lattice oxide (eV)	Std. Dev. (±eV)	%	FWHM (eV), 10 eV pass energy	FWHM (eV), 20 eV pass energy	O 1s hydroxide, hydrated or defective oxygen, organic oxygen (eV)	Std. Dev. (±eV)	%	FWHM (eV), 10 eV pass energy	FWHM (eV), 20 eV pass energy
Sc(III) oxide	529.69	0.09	72	1.06	1.11	531.28	0.15	28	2.00	1.91
Sc, thin air-formed oxide/hydrated (ScOOH)	529.57	0.05	48	1.36	1.37	531.35	0.10	52	2.04	1.94
Sc, thick air-formed oxide/fully hydrated						531.82	0.06	100	2.59	2.71
Ti(IV) oxide (rutile)	529.70	0.10	61	1.01	1.03	530.99	0.15	39	2.03	2.29
Ti(IV) oxide (anatase)	529.87	0.00	80	1.05	1.10	531.00	0.04	20	2.14	2.11
V(IV) oxide	530.48	0.04	100	1.37	1.42					
V(V) oxide	530.75	0.10	100	1.22	1.25					
Cu(I) oxide	530.20	0.01	64	1.18	1.23	531.57	0.06	36	1.28	1.28
Cu(II) oxide	529.68	0.05	68	0.86	0.89	530.99	0.07	32	1.97	1.97
Cu(II) hydroxide						531.24	0.06	100	1.58	1.59
Zn(II) oxide	529.76	0.04	70	1.00	1.05	531.25	0.05	30	1.68	1.70

$$\%\ \text{Cu(II)} = \frac{B + A1}{A + B} \times 100 = \frac{B(1 + (A1_s/B_s))}{A + B} \times 100 \qquad (2)$$

where B is the area of the shake-up peak and A is the total area of the main peak.

In order to determine accurate values of $A1_s/B_s$, seven Cu $2p_{3/2}$ analyses of pure Cu(OH)$_2$ were obtained. Analyses were carried out on the various Cu(OH)$_2$ samples at acquisition times of generally less than a few minutes as it has been shown that reduction of Cu(OH)$_2$ can occur after extended X-ray exposure [75]. Our studies suggest that after X-ray exposures of 3 h, up to 10% of Cu(OH)$_2$ has been reduced to Cu(I). At pass energies of 20 eV and 40 eV, $A1_s/B_s$ values of 1.57 ± 0.1 and 1.59 ± 0.1 were found, respectively. A similar analysis of a pure CuO sample was also carried out and gave a $A1_s/B_s$ value of 1.89 ± 0.08 (20 eV pass energy). Fig. 4 shows spectra for a sputter cleaned metal surface, CuO and Cu(OH)$_2$ standards used for $A1_s/B_s$ determination and a spectrum of the native oxide on a pure metal surface with the amount of oxidation of the surface calculated.

It should be noted that the peak-shape and main peak to shake-up peak separation is quite different for Cu(OH)$_2$ and CuO (Fig. 4). Precise curve-fitting parameters for CuO and Cu(OH)$_2$ are presented in Table 9. This is useful (along with the O 1s signal if only Cu species are present) in determining which $A1_s/B_s$ value to use for Cu(0):Cu(II) (or Cu(I):Cu(II)) calculations. If the Cu(0) or Cu(I) signal is relatively strong (and the sample is conducting) some assessment of which is present in the sample may be made based on the BE of the $2p_{3/2}$ peak. For a well calibrated spectrometer the BE for Cu(0) should be almost exact. Any deviation from this should then be due to the presence of Cu(I). Spectrometer calibration using sputter cleaned Cu metal would be appropriate when these types of analyses are carried out. If levels of Cu(II) are relatively low, it is possible to confirm the assignment of Cu(0) or Cu(I) using the Auger parameter (see Tables 7 and 8). This is also required for a non-conductive surface where charge correction to adventitious carbon will make assignment more challenging. Schoen [76] has also shown that a clear differentiation can be made using the Cu L$_3$M$_{4,5}$M$_{4,5}$ Auger spectral line-shapes. In practice, quantifying a mix of Cu(0), Cu(I) and Cu(II) species would require precise constraints on BE, FWHM, and peak-shape parameters. Resolution of these components will be difficult with larger amounts of Cu(II) compounds present due to the overlap of peaks for these three components. It may be possible to fit the $2p_{3/2}$ spectrum using a set of constrained peaks that simulate the entire peak-shape

(including the shake-up components) for the Cu(II) species present (Table 9).

3.5. Zinc

Although numerous references for the Zn $2p_{3/2}$ peak for zinc metal and oxide can be found it is generally agreed that the use of the modified Auger parameter is preferred for species identification. Wöll [77] provides an excellent review of single crystal ZnO surface work including a detailed list of C 1s and O 1s values for adsorbed species. The Zn $2p_{3/2}$ lines for Zn and ZnO are quoted at 1021.4 eV and 1021.7 eV with the O 1s for ZnO found at 530.4 eV. The author quotes a value of 530.6 eV (FWHM 1.35 eV) in a later paper [78]. No attempts at quantification of zinc metal/oxide components were found in the literature.

The Zn $2p_{3/2}$ spectrum of Zn oxide, though free from multiplet splitting and other complicating effects, suffers from an overlap with the metal peak BE (Table 10). Chemical state determination can be made using the modified Auger parameter ($2p_{3/2}$, L$_3$M$_{45}$M$_{45}$). If the Auger peak is unavailable or comprised (by, for example, overlap with the Na Auger line) the oxide peak can generally be assigned based on its larger FWHM compared to the metal. Due to the spectral overlap, mixed systems of metal and oxide will be very difficult to quantify. However in cases where the Zn metal is in electrical contact with a conductive substrate an overlayer of non-conductive oxide will charge differentially from the substrate. The action of the charge neutralization system will move the oxide peak to a lower BE separated from the metal allowing for peak area quantification.

It should be noted that is has been shown that BE and Auger parameters for Zn (as well as Cu and Ti) can change for very thin films on certain substrates (interface effects) and for very small particles (particle size effects) [79,80]. This will be an important to consider for those studying catalysis and nano-compounds.

3.6. Oxygen

The O 1s BE and FWHM values obtained for the standard samples are presented in Table 11. For many of the pure oxide samples there is a second higher BE peak that can be ascribed to contributions from a defective oxide component inherent in these oxide surfaces as suggested previously [10]. Other work has shown that this is a defective oxide peak and not hydroxide as the presence of hydroxide has been ruled out by other methods [4,81]. For all of the

oxides studied here this peak has an area contribution between 20% and 40% consistent with other powdered oxides including nickel [10] and chromium [12]. There was also no difference in this peak area between Cr_2O_3 fractured in vacuum and mounted on conductive tape. These contributions from defective sites are unlikely to compromise the assignment of chemical states. It should be noted that this second peak could result from carbonates species [1,2]. Inspection of the C 1s spectrum should confirm if this is occurring.

Pure oxide samples were not heated to remove possible surface hydroxides before analysis to avoid reduction of the oxide. In one related experiment in this laboratory with MnO heated to 600 °C for 12 h, there was no significant change in the higher BE component ascribed to defective oxide, indicating little or no surface hydroxides are present.

4. Conclusions

X-ray photoelectron spectroscopy (XPS) analysis of the 2p spectra of the first row transition metals is challenging due to peak asymmetries, complex multiplet splitting, shake-up and plasmon loss structure, and uncertain, overlapping BE positions. Practical curve-fitting procedures for the various chemical states in of Sc, Ti, V, Cu and Zn containing samples have been presented. These procedures are based on a critical evaluation of existing literature and on high-resolution analyses of well-characterized standards. The review of the current literature shows reporting of all values necessary for reproducible quantitative chemical state analysis to be lacking in a majority of cases. A full reporting of binding energies, full-width at half maximum (FWHM) values, spin-orbit splitting values, and asymmetric peak-shape fitting parameters (for conductive species) has been presented and, constrained appropriately, will allow the reader to consistently curve-fit spectra from a variety Sc, Ti, V, Cu and Zn containing compounds or surfaces. These procedures are relatively simple to implement and have been found to be consistently reproducible across a wide range of samples.

A quantification procedure for Cu species incorporating the use of the shake-up satellites for Cu(II)-containing compounds and the exact binding energies of the Cu(0) and Cu(I) peaks has been shown to be an effective method for chemical state analysis of copper surfaces. The use of the modified Auger parameter for Cu and Zn species allows for corroborating evidence when there is uncertainty in the binding energy assignment. Different charge calibration methods have been discussed. Adventitious carbon, with a binding energy set to 284.8 eV remains a good option for most samples. Charge referencing to O 1s works well for vanadium containing samples only if vanadium compounds account for the majority of the O 1s signal. It has also been shown to be possible to reference to known peak positions such as the metal or a common or well-defined oxide such as TiO_2 or V_2O_5.

Acknowledgments

Appendix I. Selected XPS survey scan results in atomic percent.

Sample	C	O	Sc	Ti	V	Cu	Zn	N	Na	Mg	P	Cl	K	Ca	Fe	Ba	Pb
Sc(III) oxide	20.3	49.0	30.6														
Sc, thin air-formed oxide/hydrated (ScOOH)	19.4	51.5	29.1														
Sc, thick air-formed oxide/fully hydrated	54.8	36.0	7.6														
Ti(IV) oxide (rutile)	16.9	55.8		17.9				0.4		2.8	2.9	0.4	2.4	0.9	1.1		
Ti(IV) oxide (anatase)	22.6	52.4		25.0													
V(IV) oxide	24.5	53.6			21.2			0.7									
V(V) oxide	20.9	56.4			22.3				0.3								
Cu(I) oxide	65.7	21.2				11.9	0.8									0.1	
Cu(II) oxide	20.3	42.5				37.1											
Cu(II) hydroxide	23.0	49.4				24.8						2.8					
Zn(II) oxide	14.6	48.3					37.1										0.4

References

[1] C.D. Wagner, A.V. Naumkin, A. Kraut-Vass, J.W. Allison, C.J. Powell, J.R. Rumble Jr., NIST Standard Reference Database 20, Version 3.4 (web version) (http://srdata.nist.gov/xps/), 2003.
[2] J.F. Moulder, W.F. Stickle, P.E. Sobol, K.D. Bomben, Handbook of X-ray Photoelectron Spectroscopy, Perkin-Elmer Corp., Eden Prairie, MN, 1992.
[3] A.P. Grosvenor, M.C. cBiesinger, R.St.C. Smart, N.S. McIntrye, Surf. Sci. 600 (2006) 1771.
[4] H.A.E. Hagelin-Weaver, J.F. Weaver, G.B. Hoflund, G.N. Salaita, J. Electron Spectrosc. Relat. Phenom. 134 (2004) 139.
[5] H.A.E. Hagelin-Weaver, J.F. Weaver, G.B. Hoflund, G.N. Salaita, J. Alloys Compd. 389 (2005) 34.
[6] R.P. Gupta, S.K. Sen, Phys. Rev. B 12 (1975) 12.
[7] R.P. Gupta, S.K. Sen, Phys. Rev. B 10 (1974) 71.
[8] M.A. Van Veenendaal, G.A. Sawatsky, Phys. Rev. Lett. 70 (1993) 2459.
[9] M. Atanasov, D.J. Reinen, J. Electron Spectrosc. Relat. Phenom. 86 (1997) 185.
[10] M.C. Biesinger, B.P. Payne, L.W.M. Lau, A. Gerson, R.St.C. Smart, Surf. Interface Anal. 41 (2009) 324.
[11] A.P. Grosvenor, B.A. Kobe, M.C. Biesinger, N.S. McIntyre, Surf. Interface Anal. 36 (2004) 1564.
[12] M.C. Biesinger, C. Brown, J.R. Mycroft, R.D. Davidson, N.S. McIntyre, Surf. Interface Anal. 36 (2004) 1550.
[13] M.C. Biesinger, B.P. Payne, B.R. Hart, A.P. Grosvenor, N.S. McIntyre, L.W.M. Lau, R.St.C. Smart, J. Phys. Conf. Ser. 100 (2008) 012025.
[14] H. Ye, X.Y. Liu, H. Hong, Mater. Sci. Eng. C 29 (2009) 2036.
[15] H. Ye, X.Y. Liu, H. Hong, Appl. Surf. Sci. 255 (2009) 8134.
[16] C.J. Powell, A. Jablonski, J. Electron Spectrosc. Relat. Phenom. 178–179 (2010) 331.
[17] S. Tougaard, Surf. Interface Anal. 26 (1998) 249.
[18] A. Frydman, D.G. Castner, M. Schmal, C.T. Campbell, J. Catal. 157 (1995) 133.
[19] B.P. Payne, A.P. Grosvenor, M.C. Biesinger, B.A. Kobe, N.S. McIntyre, Surf. Interface Anal. 39 (2007) 582.
[20] A.P. Grosvenor, B.A. Kobe, N.S. McIntyre, Surf. Interface Anal. 36 (2004) 1637.
[21] A.P. Grosvenor, J.T. Francis, B.A. Kobe, N.S. McIntyre, Surf. Interface Anal. 37 (2005) 495.
[22] A.P. Grosvenor, B.A. Kobe, N.S. McIntyre, Surf. Sci. 574 (2005) 317.
[23] D.J. Miller, M.C. Biesinger, N.S. McIntyre, Surf. Interface Anal. 33 (2002) 299.
[24] M.C. Biesinger, Unpublished Results, University of Western Ontario, London, ON, Canada, 1995–2010.
[25] N. Fairley, http://www.casaxps.com, ©Casa software Ltd., 2005.
[26] N. Fairley, CasaXPS, Personal Communication, 2007.
[27] D. Briggs, J.C. Rivière, Spectral interpretation, in: D. Briggs, M.P. Seah (Eds.), Practical Surface Analysis by Auger and X-ray Photoelectron Spectroscopy, John Wiley & Sons, Chichester, UK, 1983, p. 135.
[28] P.A.W. Van der Heide, J. Electron Spectrosc. Relat. Phenom. 164 (2008) 8.
[29] A.G. Sharpe, Inorganic Chemistry, Longman Scientific & Technical, New York, 1988, p. 574.
[30] A.R. González-Elipe, G. Munuera, J.P. Espinos, J.M. Sanz, Surf. Sci. 220 (1989) 368.
[31] T. Godfroid, R. Gouttebaron, J.P. Dauchot, P.H. Leclère, R. Lazzaroni, M. Hecq, Thin Solid Films 437 (2003) 57.
[32] J. Pouilleau, D. Devilliers, F. Garrido, S. Durand-Vidal, E. Mahé, Mater. Sci. Eng. B 47 (1997) 235.
[33] E. McCafferty, J.P. Wightman, Appl. Surf. Sci. 143 (1992) 92.
[34] R.N.S. Sohdi, A. Weninger, J.E. Davies, J. Vac. Sci. Technol. A 9 (1991) 1329.
[35] S.A. Nasser, Appl. Surf. Sci. 157 (2000) 14.
[36] M. Balaceanu, M. Briac, D. Macovei, M.J. Genet, A. Manea, D.J. Pantelica, J. Optoelectron. Adv. Mater. 4 (2002) 107.
[37] C. Massaro, P. Rotolo, F. De Riccardis, E. Milella, A. Napoli, M. Wieland, M. Textor, N.D. Spencor, D.M. Brunette, J. Mater. Sci. Mater. Med. 13 (2002) 535.
[38] K.E. Smith, V.E. Henrich, Phys. Rev. B 23 (1985) 5384.
[39] S.J. Botha, Mater. Sci. Eng. A 234 (1998) 221.
[40] L.T. Hudson, R.L. Kurtz, S.W. Robey, D. Temple, R.L. Stockbauer, Phys. Rev. B 47 (1993) 1174.
[41] R.L. Kurtz, Surface Electronic Structure and Chemisorption of Corundum Transition-metal Oxides, Ph.D. Thesis, Yale University, New Haven, CT, 1983.
[42] R.L. Kurtz, V.E. Henrich, Surf. Sci. Spectra 5 (1998) 179.
[43] R.L. Kurtz, V.E. Henrich, Surf. Sci. Spectra 5 (1998) 182.
[44] G.L. Fleming, K. Adib, J.A. Rodriguez, M.A. Barteau, H. Idress, Surf. Sci. 601 (2007) 5726.
[45] H. Pelouchova, P. Janda, J. Weber, L. Kavan, J. Electroanal. Chem. 566 (2004) 73.
[46] P.M. Jayaweera, E.L. Quah, H. Idriss, J. Phys. Chem. C 111 (2007) 1764.
[47] H. Perron, J. Vandenborre, C. Domain, R. Drot, J. Roques, E. Simoni, J.-J. Ehrhardt, H. Catalette, Surf. Sci. 601 (2007) 518.
[48] X. Tan, Q. Fan, X. Wang, B. Grambow, Eniviron. Sci. Technol. 43 (2009) 3115.
[49] A.O.T. Patrocínio, E.B. Paniago, R.M. Paniago, N.Y. Murakami Iha, Appl. Surf. Sci. 254 (2008) 1874.
[50] G. Silversmit, H. Poelman, D. Depia, N. Barrett, G.B. Marin, R. De Gryse, Surf. Interface Anal. 38 (2006) 1257.
[51] Q. Guo, S. Lee, D.W. Goodman, Surf. Sci. 473 (1999) 38.
[52] S. Hashimoto, A. Tanaka, A. Murata, T. Sakurada, Surf. Sci. 556 (2004) 22.
[53] A.F. Carley, P.R. Chalker, J.C. Riviere, M.W. Roberts, J. Chem. Soc., Faraday Trans. 83 (1987) 351.
[54] N.R. Armstrong, R.K. Quinn, Surf. Sci. 67 (1997) 451.
[55] G. Silversmit, D. Depla, H. Poelman, G.B. Marin, R. De Gryse, J. Electron Spectrosc. Relat. Phenom. 135 (2004) 167.
[56] G. Silversmit, D. Depla, H. Poelman, G.B. Marin, R. De Gryse, Surf. Sci. 600 (2006) 3512.
[57] G. Silversmit, Ghent University, Personal Communication, 2007.
[58] D. Briggs, XPS: basics principles, spectral features and qualitative analysis, in: D. Briggs, J.T. Grant (Eds.), Surface Analysis by Auger and X-ray Photoelectron Spectroscopy, IM Publications, Chichester, UK, 2003, p. 38.
[59] J. Cui, D. Da, W. Jiang, Appl. Surf. Sci. 133 (1998) 225.
[60] M. Benmoussa, E. Ibnouelghazi, A. Bennouna, E.L. Amenziane, Thin Solid Films 265 (1995) 22.
[61] E.Z. Kurmaev, V.M. Cherkashenko, Y.M. Yarmoshenko, S. Bartkowski, A.V. Postnikov, M. Neumann, L.-C. Dad, J.H. Guo, J. Nordgren, V.A. Perelyaev, W. Reichelt, J. Phys.: Condens. Matter. 10 (1998) 4081.
[62] D.H. Youn, H.T. Kim, B.G. Chae, Y.J. Hwang, J.W. Lee, S.L. Maeng, K.Y. Kang, J. Vac. Sci. Technol. A 22 (2004) 719.
[63] S.W. Goh, A.N. Buckley, R.N. Lamb, R.A. Rosenberg, D. Moran, Geochim. Cosmochim. Acta 70 (2006) 2210.
[64] S. Poulston, P.M. Parlett, P. Stone, M. Bowker, Surf. Interface Anal. 24 (1996) 811.
[65] J.C. Otamiri, S.L.T. Andersson, A. Andersson, Appl. Catal. 65 (1990) 159.
[66] P. Velásquez, D. Leinen, J. Pascual, J.R. Ramos-Barrado, P. Grez, H. Gómez, R. Schrebler, R. Del Río, R.J. Córdova, Phys. Chem. B 109 (2005) 4977.
[67] D.N. Wang, A.C. Miller, M.R. Notis, Surf. Interface Anal. 24 (1996) 127.
[68] L. Meda, G.F. Cerofolini, Surf. Interface Anal. 36 (2004) 756.
[69] L. Feng, L. Zhang, D.G. Evans, X. Duan, Colloids Surf. A 244 (2004) 169.
[70] L.J. Kundakovic, M. Flytzani-Stephanopoulos, Appl. Catal. A 171 (1998) 13.
[71] P. Salvador, J.L.G. Fierrom, J. Amador, C. Cascales, I. Rasines, J. Solid State Chem. 81 (1989) 240.
[72] M.C. Biesinger, B.R. Hart, R. Polack, B.A. Kobe, R.St.C. Smart, Miner. Eng. 20 (2007) 152.
[73] A.R. Gerson, M. Jasieniak, The effect of surface oxidation on the Cu activation of pentlandite and pyrrhotite, in: W.D. Duo, S.C. Yao, W.F. Liang, Z.L. Cheng, H. Long (Eds.), Proceedings of the XXIV International Minerals Processing Congress, Science Press Beijing, Beijing, China, 2008, pp. 1054–1063.
[74] J.F. Watts, J. Wolstenholme, An Introduction to Surface Analysis by XPS and AES, Wiley, Rexdale, 2003, p. 71.
[75] W.M. Skinner, C.A. Prestidge, R.St.C. Smart, Surf. Interface Anal. 24 (1996) 620.
[76] G. Schoen, J. Electron Spectrosc. 7 (1972) 377.
[77] C. Wöll, Prog. Surf. Sci. 82 (2007) 55.
[78] Y.K. Gao, F. Traeger, O. Shekhah, H. Idriss, C. Wöll, J. Colliod Interface Sci. 338 (2009) 16.
[79] G. Lassaletta, A. Fernádez, J.P. Espinós, A.R. González-Elipe, J. Phys. Chem. 99 (1995) 1484.
[80] J.P. Espinós, J. Morales, A. Barranco, A. Caballero, J.P. Holgado, A.R. González-Elipe, J. Phys. Chem. B 106 (2002) 6921.
[81] P.R. Norton, G.L. Tapping, J.W. Goodale, Surf. Sci. 65 (1977) 13.